AIAA 80-1441R

Numerical Study of Separated Turbulent Flow over Airfoils

A. Sugavanam* and J. C. Wu†
Georgia Institute of Technology, Atlanta, Ga.

A numerical scheme for the solution of two-dimensional time-dependent Reynolds equations is developed and applied to the flow past airfoils. The airfoil is mapped conformally into a circular cylinder, and the equations are solved in the cylinder plane. The turbulence models used in this study are the mixing-length model and a hybrid model consisting of mixing-length model and the two-equation k-ϵ model. An explicit integral relation is used to determine the kinematics of the problem. After the method was calibrated using simpler geometries, it was applied to the case of a 12% thick Joukowski airfoil at 15 deg angle of attack, at a Reynolds number of 3.6×10^6. It is observed from the results that the turbulent flow past an airfoil at high angles of attack shows oscillatory behavior (with the lift and drag coefficients continuously varying with time) similar to the behavior in laminar flows.

Introduction

MAJOR problems associated with the numerical simulation of general viscous flows are the computer resource requirements as compared with currently available computers and the lack of detailed understanding of turbulent transport processes. The problem of excessive computing needs for external flows can be alleviated substantially by using the integrodifferential approach developed by Wu et al.,[1-4] which confines the solution field to the vortical region. This method requires much less computational effort compared to other methods, since the vortical region is much smaller than the potential region. The accuracy and the solution speed of this method have been clearly demonstrated by several earlier computations.[5,6]

The problem of simulating the turbulent flow still remains unresolved. In principle, the time-dependent Navier-Stokes equations are adequate to describe the details of time-dependent eddying motions of turbulence. However, since many of the important features of turbulence are of small scale, any computational approach to solving the Navier-Stokes equations for turbulent flows would require prohibitively large computer time and data storage. None of the computers available in the foreseeable future will have the capability to solve the Navier-Stokes equations for turbulent flows. At present, the more rewarding approach to turbulent flow problems seems to be solving the time-averaged Reynolds equations. However, the process of time averaging results in unknown Reynolds stress terms that require turbulence modeling. Some turbulence models[7,8] are extremely complex to use in practice since they are still in their developmental stages. In the present work, a mixing-length model and a hybrid model consisting of a mixing-length and the two-equation k-ϵ turbulence model[9] are used.

The viscous flow past an airfoil had been of considerable interest to researchers in the past. Mehta[10] obtained the solutions for flow past a 9% thick Joukowski airfoil at an angle of attack of 15 deg and a Reynolds number of 1000. Sampath[5] obtained solutions for the same problem using the integrodifferential approach, with a considerable reduction in computer time. Thames[11] solved the flow past a NACA 0018 airfoil at an angle of attack of 10 deg and at a Reynolds number of 10,000 using a boundary-fitted coordinate system. Sankar[6] used a hybrid finite-difference and finite-element method to solve the problem of flow past an oscillating 12% thick modified Joukowski airfoil at a Reynolds number of 1000. Lately, Reddy[12] solved the flow past a NACA 0018 airfoil at zero angle of attack and at a Reynolds number of 10^6 using the integrodifferential approach with a boundary-fitted coordinate system.

All of these computations were done with the assumption of laminar flow. However, in practice, almost every flow past an airfoil involves turbulence. Thus, the primary object of this work is to develop a numerical procedure that is applicable for turbulent flows with massive separation.

In order to test the computational scheme, several calibration studies were made with simpler geometries. Subsequently this procedure was applied to the 12% thick modified Joukowski airfoil at 15 deg angle of attack for a Reynolds number of 3.63×10^6.

Mathematical Formulation

The time-averaged continuity and Reynolds equations for incompressible flow with negligible body forces are

$$\frac{\partial U_i}{\partial x_i}=0 \tag{1}$$

$$\frac{\partial U_i}{\partial t}+U_j\frac{\partial U_i}{\partial x_j}=-\frac{1}{\rho}\frac{\partial p}{\partial x_i}+\nu\frac{\partial^2 U_i}{\partial x_j\partial x_j}-\frac{\partial\overline{u_iu_j}}{\partial x_j} \tag{2}$$

where U_i is the mean velocity, ρ the density, ν the kinematic viscosity, and $-u_iu_j$ the Reynolds stress.

The curl of Eq. (2) yields the mean flow vorticity transport equation:

$$\frac{\partial\omega_i}{\partial t}=\omega_j\frac{\partial U_i}{\partial x_j}-U_j\frac{\partial\omega_i}{\partial x_j}+\nu\frac{\partial^2\omega_i}{\partial x_j\partial x_j}-\epsilon_{ijk}\frac{\partial^2}{\partial x_j\partial x_m}(\overline{u_ku_m}) \tag{3}$$

where

$$\omega_i=\epsilon_{ijk}\frac{\partial U_k}{\partial x_j} \tag{4}$$

The mean flow continuity equation (1) and the definition of vorticity, Eq. (4), with appropriate velocity boundary conditions, constitute the entire kinematics of the problem. Since

Presented as Paper 80-1441 at the AIAA 13th Fluid and Plasma Dynamics Conference, Snowmass, Colo., July 14-16, 1980; submitted Sept. 24, 1980; revision received Aug. 10, 1981.

*Postdoctoral Fellow, School of Aerospace Engineering, currently with Lockheed-Georgia Company, Marietta, Ga. Member AIAA.

†Professor, School of Aerospace Engineering. Associate Fellow AIAA.

Eqs. (1) and (4) are identical to the continuity equation and vorticity definition of instantaneous motion, the integral representations for the velocity vector previously derived for a laminar flow[13] is directly applicable to the mean velocity of turbulent flow. The integral representation written in indicial notation is[14]

$$U_i = -\frac{1}{A}\left\{\iint_R \frac{\epsilon_{ijk}\omega_{0,j}(x_0-x)_k}{[(x_0-x)_m(x_0-x)_m]^{d/2}}\mathrm{d}R_0 + \oint_B \frac{U_{0,m}(x_0-x)_m n_{0,i} - U_{0,m}(x_0-x)_i n_{0,m}}{[(x_0-x)_m(x_0-x)_m]^{d/2}}\mathrm{d}B_0 - \oint_B \frac{U_{0,m}(x_0-x)_m n_{0,m}}{[(x_0-x)_m(x_0-x)_m]^{d/2}}\mathrm{d}B_0\right\} \quad (5)$$

where B is the boundary of the region R and the subscript 0 indicates that the variables and the integrations are in the x_0 space, $n_{0,i}$ is the ith component of the outward normal unit vector, $A=4$ and $d=3$ for three-dimensional problems, and $A=2$ and $d=2$ for two-dimensional problems. For the special case of external flow problems with no-slip boundary conditions on the solid surfaces, the explicit expression for the mean velocity reduces to[15]

$$U_i = -\frac{1}{A}\int_R \frac{\epsilon_{ijk}\omega_{0,j}(x_0-x)_k}{[(x_0-x)_m(x_0-x)_m]^{d/2}}\mathrm{d}R_0 + U_{\infty,i} \quad (6)$$

At any instant of time, the vorticity is nonnegligible only within a finite distance away from the solid boundary: Eq. (6) is evaluated only over this region. The kinematic boundary conditions for the external flow problem require that the velocity reach the freestream velocity at infinite distances away from the solid surfaces. This requirement is readily satisfied by Eq. (6). However, if the Poisson equations for the kinematics are to be solved by finite-difference methods, without any coordinate transformation, this boundary condition is difficult to satisfy since the computational effort involved would be considerable.

In the kinetics of the problem, expressing the Reynolds stress in terms of the eddy viscosity ν_t and the mean strain rate yields

$$-\overline{u_j u_j} = \nu_t\left(\frac{\partial U_i}{\partial x_j} + \frac{\partial U_j}{\partial x_i}\right) \quad (7)$$

Using Eq. (7), and specializing the equations for two-dimensional flows, Eq. (3) becomes

$$\frac{\partial \omega}{\partial t} = -U_j\frac{\partial \omega}{\partial x_j} + \frac{\partial^2}{\partial x_j \partial x_j}(\nu_e \omega) + S_\omega \quad (8)$$

where ω is the only component of vorticity, ν_e is the effective viscosity defined by

$$\nu_e = \nu_t + \nu \quad (9)$$

and S_ω is the source term given by[15]

$$S_\omega = 2\left[\frac{\partial^2}{\partial x^2}\left(\nu_e\frac{\partial U}{\partial y}\right) - \frac{\partial^2}{\partial y^2}\left(\nu_e\frac{\partial V}{\partial x}\right) + \frac{\partial^2}{\partial x \partial y}\left(\nu_e\frac{\partial V}{\partial y}\right) - \frac{\partial^2}{\partial x \partial y}\left(\nu_e\frac{\partial U}{\partial x}\right)\right] \quad (10)$$

Turbulence Modeling

Time averaging the equations of motion results in more unknowns than the number of equations. This "turbulence closure" problem has to be solved through the construction of a turbulence model. Detailed descriptions of various turbulence models together with their relative merits may be found in Refs. 9 and 16. The first model used in the present study, the Prandtl mixing-length mode, expresses eddy viscosity in terms of vorticity and length scale as[17]

$$\nu_t = \kappa^2 y^2 |\omega| \quad (11)$$

where κ is the von Kármán constant, taken as 0.41 in this study, and y is the distance measured along the normal to the wall.

The mixing-length model, in spite of its simplicity, has led to satisfactory results in several internal and external attached flow problems. However, the mixing-length model fails to describe certain basic processes in turbulence, such as convection, diffusion, production, and dissipation. This discrepancy results in erroneous predictions of flowfield details in recirculating flows.[16] A turbulence model that solves a system of differential equations can accommodate the turbulence processes mentioned above. Launder and Spalding[9] compared several turbulence models and concluded that the two-equation k-ϵ turbulence model with turbulence kinetic energy k and turbulence energy dissipation rate ϵ as the model variable has better predictive capability than other models. This model defines the eddy viscosity as

$$\nu_t = c_\mu k^2/\epsilon \quad (12)$$

where k and ϵ are defined by

$$k = \frac{1}{2}\overline{u_i u_i} \text{ and } \epsilon = \nu\left(\overline{\frac{\partial u_i}{\partial x_j}\frac{\partial u_i}{\partial x_j}}\right) \quad (13)$$

The model differential equations are[9]

$$\frac{\partial k}{\partial t} = -U_j\frac{\partial k}{\partial x_j} + \frac{\partial}{\partial x_j}\left(\nu_t\frac{\partial k}{\partial x_j}\right) + \nu_t\left(\frac{\partial U_i}{\partial x_j} + \frac{\partial U_j}{\partial x_i}\right)\frac{\partial U_i}{\partial x_j} - \epsilon \quad (14)$$

$$\frac{\partial \epsilon}{\partial t} = -U_j\frac{\partial \epsilon}{\partial x_j} + \frac{\partial}{\partial x_j}\left(\frac{\nu_t}{\sigma_\epsilon}\frac{\partial \epsilon}{\partial x_j}\right) + C_1\frac{\epsilon}{k}\nu_t\left(\frac{\partial U_i}{\partial x_j} + \frac{\partial U_j}{\partial x_i}\right)\frac{\partial U_i}{\partial x_j} - C_2\frac{\epsilon^2}{k} \quad (15)$$

where for the present work

$$C_\mu = 0.09,\ C_1 = 1.44,\ C_2 = 1.92, \text{ and } \sigma_\epsilon = 1.3 \quad (16)$$

The mathematical formulation discussed above is specialized and applied to the study of incompressible turbulent flow past an impulsively started airfoil. The airfoil geometry and the grid system are generated through a conformal transformation that transforms the airfoil into a circle. The airfoil chosen for the numerical study is a modified 12% thick symmetric Joukowski airfoil. The shape of this airfoil in the complex plane $z=x+iy$ can be transformed using the conformal transformation[5]

$$z = \zeta + \gamma + \frac{C^2}{\zeta + \gamma} \quad (17)$$

into a circle of unit radius in the ζ-plane, with $\zeta = re^{i\theta}$, with C and γ as real constants. In the present problem these are taken to be 0.81278 and 0.0753423, respectively. The scale factor H of the conformal transformation is defined by

$$H = \left|\frac{\mathrm{d}z}{\mathrm{d}\zeta}\right| \quad (18)$$

The kinetic equations in the transformed plane are as follows.

Vorticity transport

$$r^2H^2\frac{\partial\omega}{\partial t}+r^2V_r\frac{\partial\omega}{\partial r}+rV_\theta\frac{\partial\omega}{\partial\theta}=r^2\frac{\partial^2}{\partial r^2}(\nu_e\omega)+r\frac{\partial}{\partial r}(\nu_e\omega)+\frac{\partial^2}{\partial\theta^2}(\nu_e\omega)+S_\omega \tag{19}$$

Turbulent kinetic energy

$$r^2H^2\frac{\partial k}{\partial t}+r^2V_r\frac{\partial k}{\partial r}+rV_\theta\frac{\partial k}{\partial\theta}=\nu_e\left(r^2\frac{\partial^2k}{\partial r^2}+r\frac{\partial k}{\partial r}+\frac{\partial^2k}{\partial\theta^2}\right)+r^2\frac{\partial\nu_e}{\partial r}\frac{\partial k}{\partial r}+\frac{\partial\nu_e}{\partial\theta}\frac{\partial k}{\partial\theta}+S_k \tag{20}$$

Turbulent energy dissipation rate

$$r^2H^2\frac{\partial\epsilon}{\partial t}+r^2V_r\frac{\partial\epsilon}{\partial r}+rV_\theta\frac{\partial\epsilon}{\partial\theta}=\left(\frac{\nu_t}{\sigma_\epsilon}+\nu\right)\left(r^2\frac{\partial^2\epsilon}{\partial r^2}+r\frac{\partial\epsilon}{\partial r}+\frac{\partial^2\epsilon}{\partial\theta^2}\right)+\frac{r^2}{\sigma_\epsilon}\frac{\partial\nu_t}{\partial r}\frac{\partial\epsilon}{\partial r}+\frac{1}{\sigma_\epsilon}\frac{\partial\nu_t}{\partial\theta}\frac{\partial\epsilon}{\partial\theta}+S_\epsilon \tag{21}$$

The source term S_ω in Eq. (19) can be ignored, since it is negligible compared with other terms in the equation. However, S_k and S_ϵ, which are the source terms in the k and ϵ equations (the sum of generation and dissipation terms), are very significant. These terms do not transform as conveniently as the diffusion and convection terms and hence are evaluated in the physical plane.

The expressions for the radial and tangential components of velocity in the transformed plane are

$$V_r=U_\infty\cos\theta-\frac{1}{2\pi}\iint_R\frac{\omega_0H_0^2r_0^2\sin(\theta-\theta_0)\,dr_0d\theta_0}{r^2+r_0^2-2rr_0\cos(\theta-\theta_0)} \tag{22}$$

$$V_\theta=-U_\infty\sin\theta+\frac{1}{2\pi}\iint_R\frac{\omega_0H_0^2r_0[r-r_0\cos(\theta-\theta_0)]\,dr_0d\theta}{r^2+r_0^2-2rr_0\cos(\theta-\theta_0)} \tag{23}$$

The surface vortex sheet strength is computed using the integral relation[5]

$$\zeta_k=\frac{1}{2\pi}\iint_{R^-}\frac{(r_0^2-1)\omega_0H_0^2r_0dr_0d\theta_0}{1+r_0^2-2r_0\cos(\theta_0-\theta)}+2U_\infty\sin\theta \tag{24}$$

where R^- is the region excluding the boundary.

Numerical Formulation

In this section the numerical treatment of the kinetics, the numerical treatment of the kinematics, and the boundary conditions are described. The numerical scheme for solving all the transport equations was kept identical for convenience. To include the separated and wake regions of the flow around the airfoil, a coordinate stretching relation of the form

$$r=e^s+c \tag{25}$$

is used. A uniform grid spacing is used in the θ direction. The resulting differential equations are approximated by a time-implicit finite-difference equation using backward differencing to represent the time derivative. Space derivatives in the diffusion and source terms are represented by a central differencing at the new time level. The central differencing of the space derivatives in the convection terms results in spurious values of transport quantities.[18] Thus, a second-order upwind differencing scheme[19] is used for the convection terms. The finite-difference form of a general transport quantity f reduces to

$$A_{i,j}f_{i,j-1}^{n+1}+B_{ij}f_{i-1,j}^{n+1}+D_{i,j}f_{i+1,j}^{n+1}+E_{i,j}f_{i,j+1}^{n+1}+F_{i,j}f_{i,j}^{n}=C_{i,j}f_{i,j}^{n+1} \tag{26}$$

where $A_{i,j}$, $B_{i,j}$, $C_{i,j}$, $D_{i,j}$, $E_{i,j}$, and $F_{i,j}$ are the coefficients of the transport quantity f and may be found in Ref. 15.

Equation (26) is solved iteratively, using a "point successive underrelaxation" technique with the relaxation parameter β as follows:

$$f_{i,j}^*=\frac{1}{C_{i,j}}(A_{i,j}f_{i,j-1}^{n+1}+B_{i,j}f_{i-1,j}^{n+1}+D_{i,j}f_{i+1,j}^{n+1}+E_{i,j}f_{i,j+1}^{n+1}+F_{i,j}f_{i,j}^{n}) \tag{27}$$

$$(f_{i,j}^{n+1})^{p+1}=\beta f_{i,j}^*+(1-\beta)(f_{i,j}^{n+1})^p \tag{28}$$

where p is the iteration counter.

The kinematic computations involve evaluation of the integrals in equations for the velocities and the surface vortex sheet strengths. Direct numerical evaluation of these integrals, however, gives rise to large roundoff errors due to the fine grid used in the radial direction close to the surface of the solid. In order to eliminate this inaccuracy, a finite Fourier series approach is used. The quantity $\omega_0H_0^2dr_0$, corresponding to the radial distance r_0, is approximated by a finite Fourier series in the θ direction with a period 2π as given below.

$$F(\theta_0)=\omega_0H_0^2dr_0=\frac{a_0}{2}+\sum_{n=1}^{N-1}(a_n\cos n\theta_0+b_n\sin n\theta_0)+\frac{a_N}{2}\cos N\theta_0 \tag{29}$$

where a_0, a_n, and b_n are the Fourier coefficients of the N-term Fourier expansion given by[20]

$$a_n=\frac{1}{N}\sum_{p=0}^{2N-1}F(\theta_{0p})\cos n\theta_{0p}\qquad n=0,1,\ldots,N \tag{30}$$

and

$$b_n=\frac{1}{N}\sum_{p=0}^{2N-1}F(\theta_{0p})\sin n\theta_{0p}\qquad n=1,2,\ldots,N-1 \tag{31}$$

On substitution and integration the tangential velocity expression reduces to

$$V_\theta(r,\theta)=-U_\infty\sin\theta+\frac{1}{2}\sum_{r_0}\sum_n(a_n\cos n\theta+b_n\sin n\theta)\times\left(\frac{r}{r_0}\right)^{n-1}\quad\text{for }\frac{r}{r_0}<1$$

$$=-U_\infty\sin\theta-\frac{a_0}{2}\left(\frac{r_0}{r}\right)-\frac{1}{2}\sum_{r_0}\sum_n(a_n\cos n\theta+b_n\sin n\theta)\left(\frac{r_0}{r}\right)^{n+1}\quad\text{for }\frac{r}{r_0}>1 \tag{32}$$

Similar expressions are derived for the radial component of velocity and the surface vortex sheet strength.

The numerical implementation of the boundary conditions is very critical for turbulent flows because of the large gradients of the turbulent quantities near the surface. The structure of a turbulent boundary layer near the wall essentially consists of a very narrow viscous sublayer, an inertial layer, and an outer layer. The velocity profile is linear

in the viscous sublayer, logarithmic in the inertial layer, and a slowly varying function in the outer layer. An extremely fine grid is needed to obtain the details in the viscous sublayer. Since it is impractical, from computational time and storage considerations, to have such a mesh system, the "law of the wall" boundary conditions are used in the present study. The surface vortex sheet ζ is considered to represent the total integrated vorticity within a layer of fluid surrounding the surface thickness Δn. With the known vortex sheet strength ζ at a particular boundary location, the following relations are used to determine the friction velocity u_* at that location and then the values of ω, k, and ϵ at a data point M located at a normal distance n_M from the boundary locations.[14]

$$\zeta = -10u_* + \frac{u_*}{\kappa} \ell n\left(\frac{10\nu}{u_* \Delta n}\right) \tag{33}$$

$$\omega_M = u_*/\kappa n_M \tag{34}$$

$$\epsilon_M = u_*^3/\kappa n_M \tag{35}$$

$$k_M = u_*^2/\sqrt{C_\mu} \tag{36}$$

where the friction velocity u_* is defined as

$$u_* = (\tau_0/\rho)^{1/2} \tag{37}$$

where τ_0 is the wall shear stress at the boundary location.

The details of the solution procedure are identical to the one reported in Ref. 14. The computation is initiated with prescribed values of ω, k, and ϵ at the previous time level. In the present work, the fluid is considered to be initially at rest and is in contact with solid surface also initially at rest. The velocity of the solid surface rises suddenly to some finite value at time $t = 0$ and remains steady thereafter.

Results and Discussion

The computation procedure developed above was calibrated considering several simpler flow situations. The details of the numerical results for many of these cases are reported elsewhere.[14,21,22] In this paper, numerical results obtained for two additional test cases—1) turbulent flow past a circular cylinder and 2) turbulent flow past a Joukowski airfoil at zero angle of attack—are presented.

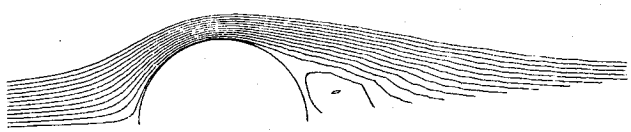

Fig. 1 Mean streamline contour for turbulent flow past a circular cylinder.

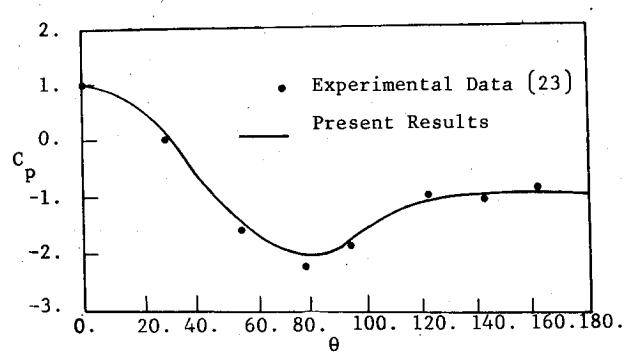

Fig. 2 Surface-pressure distribution for turbulent flow past a circular cylinder.

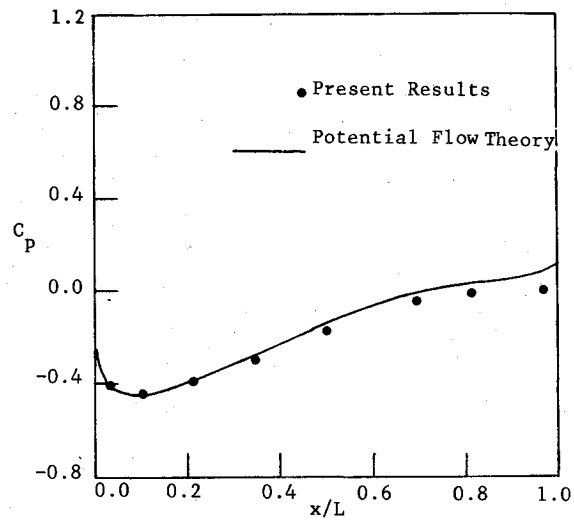

Fig. 3 Surface-pressure distribution for turbulent flow past an airfoil at zero angle of attack.

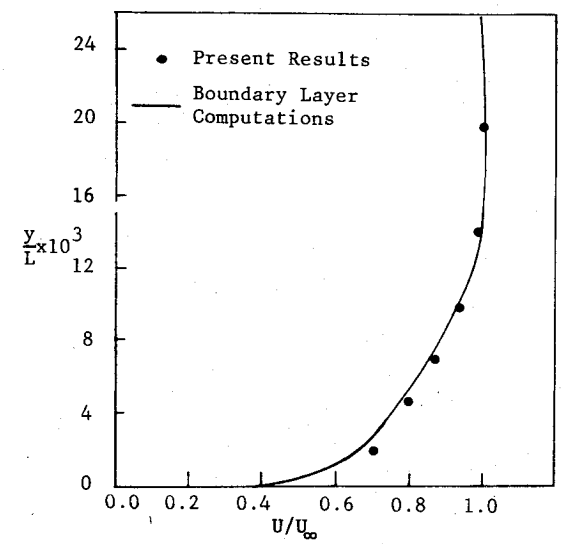

Fig. 4 Midchord mean velocity profile for turbulent flow past an airfoil at zero angle of attack.

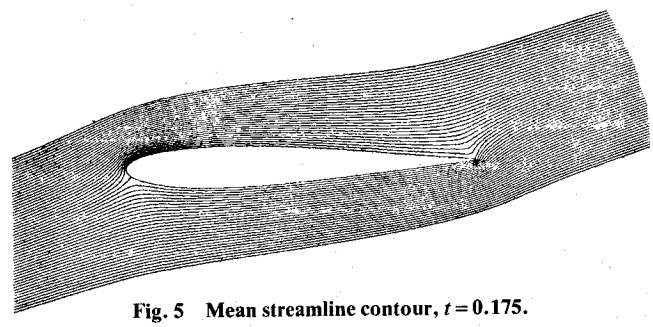

Fig. 5 Mean streamline contour, $t = 0.175$.

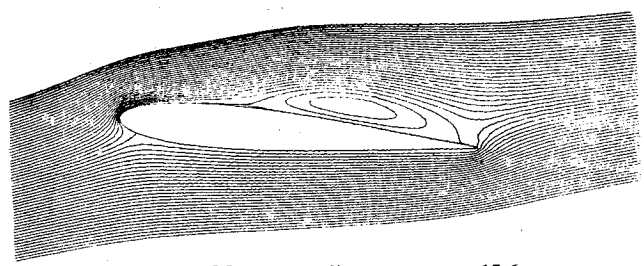

Fig. 6 Mean streamline contour, $t = 15.6$.

Case 1. Turbulent Flow past a Circular Cylinder

Turbulent flow past a circular cylinder is considered at a Reynolds number of 3.6×10^6, based on the cylinder diameter. The flow is assumed to be symmetrical about the diameter parallel to the freestream direction. The computational domain was divided into a finite-difference grid of 1200 nodes. The time-dependent computations were carried out until steady state was achieved. Figure 1 shows the mean streamline pattern for turbulent flow past a circular cylinder at the steady-state limit. The figure shows the boundary-layer growth on the forward half of the cylinder as well as the recirculating flow downstream of the cylinder. The separation occurs after the shoulder at 122 deg from the front stagnation point in the present computations. Achenbach's measurements[23] for the circular cylinder indicate that the separation occurred at 115 deg from the forward stagnation point. Figure 2 shows the experimental and computational pressure distributions. The agreement between them is good. The pressure peak occurs around 85 deg from the front stagnation point, following which the pressure gradient becomes adverse.

Case 2. Turbulent Flow past an Airfoil at Zero Angle of Attack

The computational procedure developed is applied to the case of turbulent flow past a 12% thick Joukowski airfoil at zero angle of attack. The Reynolds number considered is 3.63×10^6, based on the airfoil chord length. (The length of the airfoil based on the circular cylinder radius is 3.63 and, thus, the Reynolds number chosen corresponds to a Reynolds number of 10^6, based on the circular-cylinder radius.) All quantities are normalized with reference to the freestream velocity and the circular-cylinder radius.

The computations were initiated with an impulsive start. At a nondimensional time of 7.4, a steady state was determined to have been reached based on the agreement of computed surface vorticity values with previous time levels within 1%.

Figure 3 shows the surface-pressure distribution over the chord length. The pressure peak is near the maximum thickness point, as anticipated. Also shown in the figure is the potential-flow pressure distribution. Present results agree very well with the potential-flow results. Figure 4 compares the computed midchord mean velocity profile with that computed using a turbulent boundary-layer theory,[24] using the turbulence model developed by Cebeci and Smith.[25] These two computed velocity profiles are seen to agree very well. The two-equation k-ϵ model is well tested for boundary-layer-type flows. Thus, it is not surprising that the potential-flow and boundary-layer results agree very well with the present computational procedure.

Case 3. Turbulent Flow past an Airfoil at Finite Angle of Attack

The procedure was next applied to the flow past an airfoil at stall. As earlier, the modified 12% thick Joukowski airfoil is considered at an angle of attack of 15 deg. In the transformed circular-cylinder plane a grid was chosen with 1800 nodes. An exponential stretching relation was used in the radial direction and a uniform grid spacing was used in the θ direction. The computational boundary extended roughly to eight chord lengths in the airfoil plane. (As before, all quantities are nondimensionalized with reference to the freestream velocity and the circular-cylinder radius.) The time increments varied from $\Delta t=0.005$ to $\Delta t=0.08$. A total of 500 time steps were used to march to a time level of 37.2. (The computer time taken per time step was roughly 60 s in CYBER 74-6400 CPU.)

Convergence problems can be encountered using the two-equation k-ϵ model. This model is known to predict improper values of turbulent kinetic energy in certain flow situations.[26] Thus, in the initial time levels the mixing-length model was used. At later time levels a hybrid model consisting of both the mixing-length model and the k-ϵ model was used in different parts of the flowfield. The mixing-length model was used very close to the wall (0.12 rad away from the circular cylinder), and the k-ϵ model was used in the rest of the region.

The first stage of flow development reflects the effects of the impulsive start. At time $t=0$, the vorticity exists only at the surface of the airfoil and the flow away from the surface is potential. The rear stagnation point is located at the upper surface of the airfoil. Within a short time, the rear stagnation point moves close to the trailing edge. This movement is associated with the formation of a starting vortex. Figure 5 shows the mean streamline pattern at a time level of $t=0.175$. At further time levels the boundary layer grows on the airfoil, and the boundary-layer thickness on the upper surface is greater than that on the lower surface, due to the presence of the strong adverse pressure gradient on the upper surface.

The second stage of flow development describes the occurrence of separation together with the formation and growth of the "primary bubble." Separation occurs around a time level of 5 near the trailing edge, and the presence of the bubble is observed around a time level of 6. Figure 6 shows the growth of the "primary bubble." With an increase in time, more and more closed mean streamlines are observed inside the bubble. The lift coefficient increases with the increasing size of the primary bubble.

In the third stage of flow development, the primary bubble is ruptured and an open "burst bubble" is formed (Fig. 7). Also, at this time level two additional bubbles (one near the leading edge and one near the trailing edge) are observed. For convenience these are referred to as the "secondary bubble" and the "trailing edge bubble." At subsequent time levels

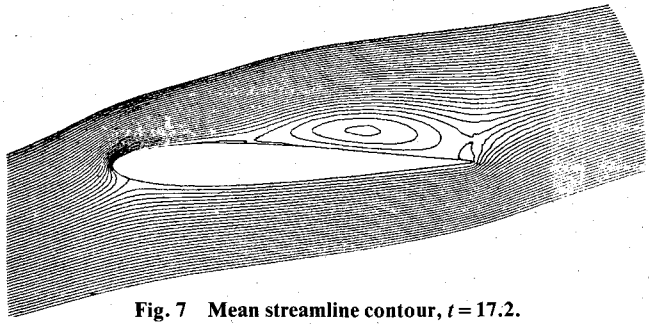

Fig. 7 Mean streamline contour, $t=17.2$.

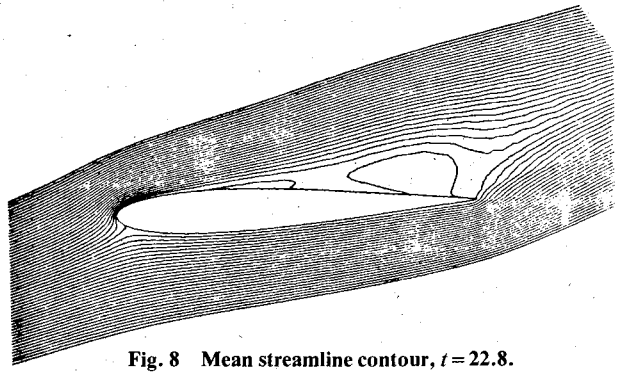

Fig. 8 Mean streamline contour, $t=22.8$.

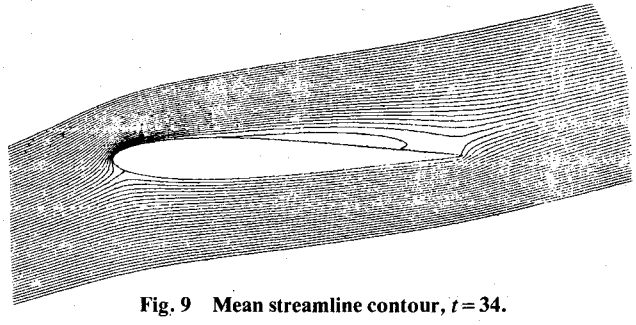

Fig. 9 Mean streamline contour, $t=34$.

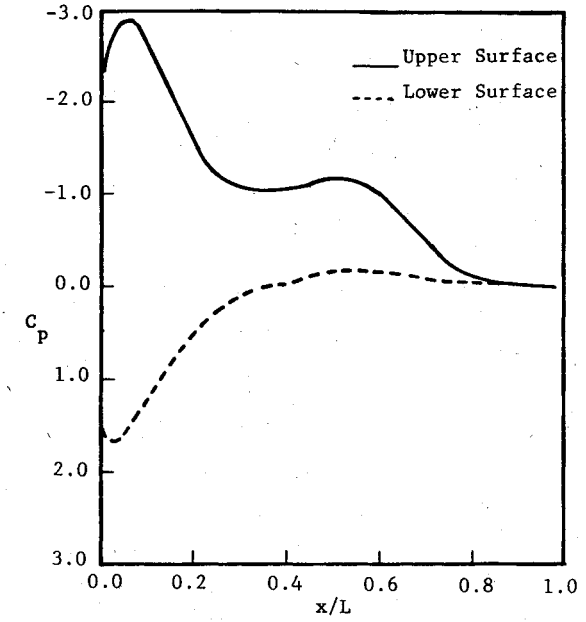

Fig. 10 Surface-pressure distribution on the airfoil, $t = 9.2$.

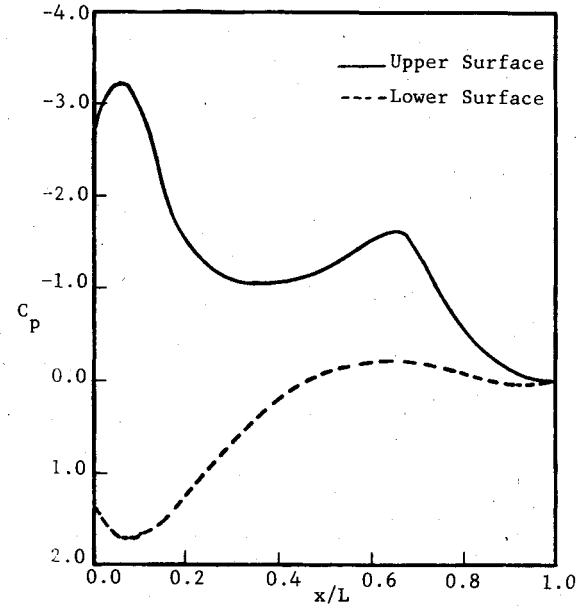

Fig. 11 Surface-pressure distribution on the airfoil, $t = 15.6$.

there is a complex interaction (Fig. 8) between the burst primary bubble and the trailing edge bubble. During this interaction the lift coefficient drops.

The fourth stage of flow development involves the growth of the secondary bubble. At a time level of 26, the wake and the boundary layer near the trailing edge are very thick. The rate of expansion of the secondary bubble is very slow. At a time level of 34 (Fig. 9), the secondary bubble looks very much like the initial primary bubble. Also, with the increase in size of the secondary bubble, the lift coefficient increases.

Figures 10 and 11 show the pressure distribution over the airfoil at time levels 9.2 and 15.6. An appropriate integration of pressure and the skin friction distribution yields the forces on the airfoil. Figure 12 shows the time histories of the lift and drag coefficients. The maximum lift coefficient 1.54 occurs at a time level of 15.6, whereas the minimum lift coefficient 0.56 occurs at a time level of 26. The drag coefficient, on the other hand, varies from 0.22 to 0.42, and their extrema occur at time levels 12 and 27. Critzos et al.[27] conducted an experiment with flow past a NACA 0012 airfoil at a Reynolds number of

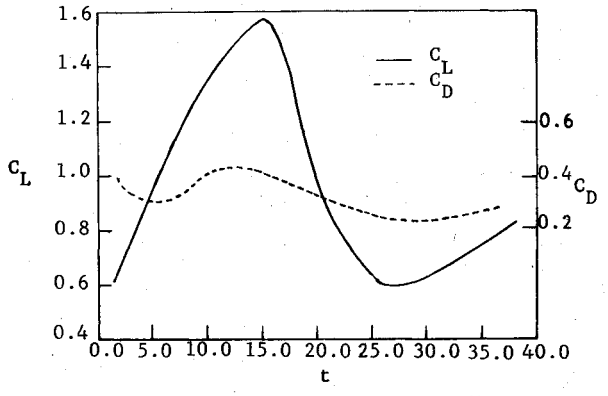

Fig. 12 Time histories of lift and drag coefficients.

1.8×10^6 based on the chord. The measurements show that the airfoil stalled at an angle of attack of 15 deg, and the measured lift and drag coefficients at those conditions were 1.26 and 0.28. Their experiments did not indicate oscillatory behavior of lift and drag, as observed in this study. However, the experimental lift and drag coefficients fall within the range predicted by the present calculations.

The prime motivation of this study was to develop the computational capability for studying complex external turbulent flows. The present results indicate that it is possible to obtain satisfactory turbulent flow solutions past complex geometries, using acceptable computer time with widely accessible computers, provided there is a suitable turbulence model. Improved turbulence models are required in the transitional and recirculating regions. Additional extensive experimental data are needed to establish the accuracy and range of application of turbulence models for general viscous flows.

Acknowledgments

This research is supported by the U.S. Army Research Office under Grant DAA-G29-75-G-0147. The work discussed is based in part on the first author's Ph.D. Thesis at Georgia Institute of Technology. Financial support by the Lockheed-Georgia Company during the later part of his Ph.D. studies is acknowledged.

References

[1] Wu, J. C. and Thompson, J. F., "Numerical Solution of Time-Dependent Incompressible Navier-Stokes Equations Using an Integro-Differential Formulation," *Computers and Fluids*, Vol. 1, 1973, pp. 197-215.

[2] Wu, J. C., "Prospects for the Numerical Solution of General Viscous Flow Problems," *Proceedings of the Viscous Flow Symposium*, Lockheed-Georgia Co., Marietta, Ga., 1976.

[3] Wu, J. C., Spring, A. H., and Sankar, N. L., "A Flowfield Segmentation Method for the Numerical Solution of Viscous Flow Problems," *Lecture Notes in Physics*, Vol. 35, 1974, pp. 452-457.

[4] Wu, J. C., "Numerical Boundary Conditions for Viscous Flow Problems," *AIAA Journal*, Vol. 14, Aug. 1976, pp. 1042-1049.

[5] Sampath, S., "A Numerical Study of Incompressible Viscous Flow around Airfoils," Ph.D. Thesis, Georgia Institute of Technology, Atlanta, Ga., Sept. 1977.

[6] Sankar, N. L., "Numerical Study of Unsteady Flow Over Airfoils," Ph.D. Thesis, Georgia Institute of Technology, Atlanta, Ga., Nov. 1977.

[7] Hanjalic, K. and Launder, B. E., "A Reynolds Stress Model of Turbulence and Its Applications to Asymmetric Shear Flows," *Journal of Fluid Mechanics*, Vol. 52, Pt. 4, 1972, pp. 609-638.

[8] Ferziger, J. H., "Large Eddy Numerical Simulations of Turbulent Flows," *AIAA Journal*, Vol. 15, Sept. 1972, pp. 1261-1267.

[9] Launder, B. E. and Spalding, D. B., "The Numerical Computation of Turbulent Flows," *Computer Methods in Applied Mechanics and Engineering*, Vol. 3, 1974, pp. 269-288.

[10] Mehta, U. B., "Starting Vortex, Separation Bubbles and Stall—A Numerical Study of Laminar Unsteady Flow around an Airfoil," Ph.D. Thesis, Illinois Institute of Technology, Chicago, Ill., 1972.

[11] Thames, F. C., "Numerical Solution of the Incompressible Navier-Stokes Equations about Arbitrary Two-Dimensional Bodies," Ph.D. Thesis, Mississippi State University, Mississippi State, Miss., May 1975.

[12] Reddy, R. N., "Numerical Solution of Incompressible Navier-Stokes Equations in Integro-Differential Formulation Using Boundary-Fitted Coordinate System," Ph.D. Thesis, Mississippi State University, Mississippi State, Miss., Aug. 1977.

[13] Wu, J. C. and Sampath, S., "A Numerical Study of Viscous Flow around an Airfoil," AIAA Paper 76-337, July 1976.

[14] Wu, J. C. and Sugavanam, A., "A Method for the Numerical Solution of Turbulent Flow Problems," *AIAA Journal*, Vol. 16, Sept. 1978, pp. 948-955; also, *Proceedings of the 3rd AIAA Computational Fluid Dynamics Conference*, 1977, pp. 168-175.

[15] Sugavanam, A., "Numerical Study of Separated Turbulent Flow Over Airfoils," Ph.D. Thesis, Georgia Institute of Technology, Atlanta, Ga., Aug. 1979,

[16] Launder, B. E. and Spalding, D. B., *Mathematical Models of Turbulence*, Academic Press, New York, 1972.

[17] Schlichting, H., *Boundary Layer Theory*, translated by J. Kestin, McGraw-Hill, New York, 1968.

[18] Gosman, A. D., "Introduction to Numerical Calculation of Recirculating Flows," *Turbulent Recirculating Flow—Prediction and Measurement*, College of Engineering, The Pennsylvania State University, 1975.

[19] Roache, P. J., *Computational Fluid Dynamics*, Hermosa Publishers, Albuquerque, N.M., 1972.

[20] Hamming, R. W., *Numerical Methods for Scientists and Engineers*, McGraw-Hill, New York, 1973.

[21] Wu, J. C., Wahbah, M. M., and Sugavanam, A., "Some Numerical Solutions of Turbulent Flow Problems by the Use of Integral Representations," *Proceedings of the Symposium on Applications of Computer Methods in Engineering*, Vol. II, 1977, pp. 983-992.

[22] Wu, J. C., Wahbah, M. M., and Sugavanam, A., "Numerical Solution of Unsteady Flow Problems Using Integro-Differential Approach," *Nonsteady Fluid Dynamics*, American Society of Mechanical Engineers, New York, 1978, pp. 245-252.

[23] Achenbach, E., "Distribution of Local Pressure and Skin-Friction around a Circular Cylinder in a Cross-Flow up to $Re = 5 \times 10^6$," *Journal of Fluid Mechanics*, Vol. 34, Pt. 4, 1968, pp. 625-639.

[24] Kottapalli, S.B.R., "Drag on an Oscillating Airfoil in a Fluctuating Free-Stream," Ph.D. Thesis, Georgia Institute of Technology, Atlanta, Ga., Aug. 1977.

[25] Cebeci, T. and Smith, A.M.O., *Analysis of Turbulent Boundary Layers, Applied Mathematics and Mechanics*, Vol. 15, Academic Press, New York, 1974.

[26] Deshpande, M. D. and Giddens, D. P., "Turbulent Entrance Flow Using a Two-Equation Model," *Physics of Fluids*, Vol. 21, Pt. 3, 1978, pp. 510-512.

[27] Critzos, C. C., Heyson, H. H., and Boswinkle, R. B. Jr., "Aerodynamic Characteristics of NACA 0012 Airfoil Section at Angles of Attack from 0° to 180°," NACA TN 3361, 1961.